Journal of Food Engineering 406 (2026) 112810

Contents lists available at ScienceDirect

Journal of Food Engineering

journal homepage: www.elsevier.com/locate/jfoodeng

Enhancing drying efficiency and temperature uniformity during microwave-assisted freeze drying: A weight-dependent microwave power approach

Isabel Kalinke [a,b,*], Günther Unterbuchberger [a,b], Ulrich Kulozik [b]

[a] Food Process Engineering, Department Life Science Engineering, TUM School of Life Sciences, Technical University Munich, Freising, Germany
[b] Food and Bioprocess Engineering, Department Life Science Engineering, TUM School of Life Sciences, Technical University Munich, Freising, Germany

ARTICLE INFO

Keywords:
Microwave power
Freeze drying
Process control
Electrification
Sustainability

ABSTRACT

Microwave-assisted freeze-drying (MWFD) presents a promising time- and energy-saving alternative to conventional, costly freeze drying. However, achieving temperature uniformity during the drying process remains a significant challenge. This study introduces a novel process control strategy designed to enhance temperature uniformity without compromising time- and energy-efficiency. Traditional MWFD methods employ a constant microwave power input, often resulting in uneven processing and potential quality loss. In contrast, our newly developed strategy adjusts the power input according to the drying progress of the sample by a weight-based approach, with increased initial microwave power input compensating for reduced power at the end of drying. Our approach demonstrated for a wide range of tested microwave input power levels significant advantages over the traditional constant power input approach. This included faster drying times, lower overall energy consumption and lower total microwave energy use. A consequent reduction in temperature non-uniformity compared to the constant power counterpart was achieved at substantially lower final product temperatures. The findings suggest that this strategy can significantly improve MWFD processes, making it a valuable alternative to traditional MWFD. This advancement is particularly relevant in the context of growing efforts towards energy and time efficiency in the food industry.

1. Introduction

Freeze-drying is a well-established preservation technique widely used in the pharmaceutical and food industries for stabilizing heat-sensitive products such as vaccines, biologics, and high-value food products (Ambros et al., 2018; Li et al., 2014; Ozcelik et al., 2019b; Sarciaux et al., 1999; Tang and Pikal, 2004). Its ability to maintain structural integrity, nutritional value, and sensory attributes is primarily attributed to the low-temperature, low-pressure environment that minimizes thermal and oxidative degradation. However, conventional freeze-drying is inherently time- and energy-intensive due to the limited heat transfer through the dried product layer, often resulting in process durations extending over several hours or days.

Microwave freeze-drying (MWFD) has emerged as a promising alternative, offering significant reductions in drying time (Abbasi and Azari, 2009; Ambros et al., 2018; Gitter et al., 2018; Jiang et al., 2013a; Ozcelik et al., 2019b), and energy consumption (Jiang et al., 2013a; Ozcelik et al., 2019b; Sunderland, 1980). Notably, the application of microwaves in freeze-drying can not only maintain but even enhance product quality, preserving critical attributes more effectively than in conventional freeze-drying (Ambros et al., 2018; Ozcelik et al., 2019a; Zhang et al., 2006b). Conventional freeze-drying heats the product from the surface using conduction or infrared radiation. In contrast, MWFD heats the product from the inside using microwaves. This volumetric heating of microwaves is particularly advantageous for low-conductivity products, in which slow heat transfer from the surface to the centre limits the drying efficiency in conventional freeze-drying.

Food products, where this challenge of low thermal conductivity is most severe, are foamed fruit and vegetable purées that have gained increasing popularity in the past years (Qadri et al., 2020b). So-called foam-mat drying has been reported amongst others, for apple (Raharitsifa and Ratti, 2010; Valenzuela and Aguilera, 2013) banana

* Corresponding author. Technical University Munich, TUM School of Life Sciences, Department Life Science Engineering, Food Process Engineering, Weihenstephaner Berg 1, 85354 Freising, Germany.
E-mail address: isabel.kalinke@tum.de (I. Kalinke).

https://doi.org/10.1016/j.jfoodeng.2025.112810
Received 24 March 2025; Received in revised form 14 August 2025; Accepted 6 September 2025
Available online 8 September 2025
0260-8774/© 2025 The Authors. Published by Elsevier Ltd. This is an open access article under the CC BY-NC license (http://creativecommons.org/licenses/by-nc/4.0/).

(Sankat and Castaigne, 2004), papaya (Qadri et al., 2020a), muskmelon (Asokapandian et al., 2016), tomato (Kadam and Balasubramanian, 2011; Rzepecka et al., 1976), and raspberry foam (Ozcelik et al., 2019a). These foams are often stabilised by maltodextrin addition (Qadri et al., 2020b). The foaming process significantly increases the surface area, thereby reducing mass transfer resistance and accelerating drying. Moreover, it enables the development of novel product structures with enhanced rehydration properties, improved retention of volatile compounds, and superior aroma release during consumption—features particularly desirable in fruit/vegetable snack applications. However, the high porosity inherent to such foams results in low thermal conductivity, posing a challenge to efficient heat transfer during foam-mat drying by conventional means of heat delivery. Consequently, the application of microwave energy has been reported as particularly beneficial for these foamed systems, offering both reduced drying times and improved final product quality (Ozcelik et al., 2019a, 2019b; Qadri et al., 2020a; Rzepecka et al., 1976). The combination of foaming and microwave technologies offers a synergistic approach that combines the benefits of both methods while potentially mitigating their individual limitations.

Despite many benefits, MWFD remains rarely used at the industrial scale. Commercial systems are available, yet adoption is hindered by limited operational experience, especially on a bigger industrial scale, and concerns over microwave-induced inhomogeneities in heat distribution. Namely, in foam-mat MWFD, non-uniformity was reported as main challenge, particularly at higher microwave power levels, as observed for raspberry foam (Ozcelik et al., 2019b). However, scientific studies addressing process control to improve uniformity in MWFD are scarce (Jiang et al., 2013b; Kalinke et al., 2024; Kalinke and Kulozik, 2023, 2024; Sickert et al., 2023a, 2023b). This research is crucial, as MWFD differs significantly from other microwave drying processes: Localised overheating can easily lead to exceeding of the glass transition temperature, resulting in structural collapse, melting, or even explosive disintegration of the sample. Sensor integration for real-time temperature monitoring is complicated by vacuum conditions, low product temperatures, sample movement, and the electromagnetic field, making process control challenging or impossible. Additional differences are the high microwave power penetration depth (Duan et al., 2012; Sickert et al., 2023b), because free water in food is fully frozen during MWFD. Further, the low-pressure environment increases the risk of undesirable plasma formation (Ambros et al., 2018; Duan et al., 2010).

Temperature non-uniformity is closely linked to microwave power input: while high power accelerates MWFD (Abbasi and Azari, 2009; Ambros et al., 2018; Duan et al., 2010; Kalinke et al., 2024; Ozcelik et al., 2019a; Ozkan et al., 2007; Wang et al., 2009; Wang and Xi, 2005), it also increases the risk of uneven temperature distribution (Kalinke et al., 2024). Conversely, reducing power improves uniformity but extends drying time. Longer drying increases operation times of the dryer equipment, consequently energy consumption of MWFD is increased (Ambros et al., 2018; Jiang et al., 2013a; Kalinke et al., 2024; Kalinke and Kulozik, 2024). Recent studies employ temperature-controlled MWFD, where power is reduced upon reaching a preset product temperature. Temperature-controlled drying is usually applied to prevent excessive product temperatures at the end of MWFD (Ambros et al., 2018; Jiang et al., 2010; Kalinke and Kulozik, 2024; Wang et al., 2009). However, it was also found to be beneficial in mitigating the rapidly increasing process inhomogeneity at the end of the MWFD process (Kalinke et al., 2024). Previous studies identified the transition from sublimation to desorption drying as the critical step of increasing temperature inhomogeneity in MWFD (Jiang et al., 2013b; Kalinke et al., 2024; Kalinke and Kulozik, 2024). Accordingly, reducing the microwave input power towards the end of the drying process, and thus during the critical transition step of the sample, was found to be advantageous for achieving more homogeneous drying in temperature-controlled MWFD.

However, effective temperature-controlled drying requires reliable in-process temperature monitoring. As mentioned before, reliable online temperature measurement is complicated. It is often restricted to specific product placements or configurations, and in many cases, entirely absent in the MWFD plant. Retrofitting such systems post-construction is typically difficult or even unfeasible (Kalinke et al., 2022). Furthermore, in many temperature-controlled MWFD processes, temperature-control is seen as a safety measure to mitigate excessive product temperatures. With this, the set maximum product temperature is often not even reached (Ambros et al., 2018). In such cases, temperature control cannot improve temperature uniformity.

The aim of this study was to address this conflict by introducing a novel power control strategy that tackles temperature inhomogeneity more reliably. For this, microwave power input was constantly reduced along drying. In the present study, this was realised by adjusting it in response to the current sample weight. To implement this, microwave power input was maintained regarding 'Watt per gram of current sample weight' [W/g current weight]. Consequently, absolute microwave power input was adjusted in discrete time intervals of 1 s in response to the real-time weight measurement of the sample. As a result, absolute microwave power input was gradually reduced as weight loss progressed during drying. Based on the decreasing drying rate with increasing drying progression (Pikal, 1994), the microwave power input was rapidly reduced during the initial sublimation drying stage and more gradually during the final desorption drying stage. This contrasted with established MWFD, where microwave power input, though often expressed as W/g, refers to a constant power input level based on the initial sample weight (e.g., 'Watt per gram of initial sample weight') (Ambros et al., 2018; Duan et al., 2010; Jiang et al., 2013a; Ozcelik et al., 2019a). In such cases, the specific microwave input power in 'Watt per gram of current sample weight' steadily increases due to mass reduction along drying. In this study, both microwave power approaches were compared for maltodextrin foam samples resembling foam-mat MWFD of fruit and vegetable purees —a food type where MWFD shows high potential due to the present severe heat transfer limitations in the product.

The advantage of the weight-dependent approach lies in its compatibility with most drying systems, which typically monitor drying progress inline via integrated weighing systems. Even in the absence of inline weighing, this approach links power control to the product's progress in drying, i.e. moisture removal—a variable that is always tracked in any form in every drying process.

Duan et al. (2012) investigated the effect of stepwise microwave power reduction during MWFD on apple crisps. They tested a power approach with three subsequent power intervals based on changes in the dielectric properties of the product: 2 h at 3.5 W/g, 2.5 h at 2.5 W/g, and 1.5 h at 1.5 W/g. This was compared to a constant power approach at 2.5 W/g. All power settings referred to 'Watt per gram of initial sample weight'. The authors found equal drying times for both power approaches. However, the variable power approach improved product quality by preventing end-stage overheating. Neither energy efficiency nor temperature uniformity were subject of their study and only one variable power approach setting was tested. While these results are promising in light of the continuous power reduction strategy proposed in this study, the approach from Duan et al. (2012) required labour-intensive preliminary assessment of dielectric properties at various drying stages. This involved repeated drying and sampling at multiple time points, followed by external dielectric analysis under the correct moisture and temperature conditions of the sample. Although effective, the method is impractical for broader application due to its complexity, laboriousness, and limited flexibility. Consequently, the investigation of a steady microwave power reduction in the proposed form of our systematic study addresses a persisting knowledge gap.

Our study was based on the following two hypotheses.

1) High absolute power levels at the beginning of drying compensate for lower microwave power input towards the end of drying. This results in drying durations and microwave energy demands comparable to

MWFD at a constant microwave power input, i.e. the state-of-the-art MWFD procedure.
2) Lower microwave power input towards the end of drying leads to an improved temperature uniformity and lower final product temperature of MWFD.

This study aims to offer a new strategy for energy-efficient and uniform MWFD, addressing the current trade-off between both aspects. By tackling existing challenges and by elucidating the largely unquantified effect of inhomogeneity in MWFD, it aims to advance the adoption of MWFD in the food industry.

2. Material and methods

2.1. MWFD experiments

2.1.1. Sample

The freeze-drying experiments were conducted using frozen maltodextrin foam samples, prepared as follows: The formulation consisted of 6.0 % w/w polysorbate 80 (Tween 80, Gerbu Biotechnik GmbH, Heidelberg, Germany), 25 % w/w maltodextrin DE-6 (Nutricia GmbH, Erlangen, Germany), and 69 % w/w deionized water. The resulting solution was whipped at 220 rpm for 15 min using a planetary mixer (KitchenAid Artisan 5KSM150, Whirlpool Corp., Greenville, USA; whisk geometry: K45WW, Whirlpool Corp., Greenville, USA).

The samples of 120 g had a cylindrical shape with a diameter of 22.5 cm and a height (foam layer thickness) of approximately 1.8 cm. They were frozen inside a covered glass Petri dish (Duran, Merck, Darmstadt, Germany) at −80 °C overnight (Freeze BF-U538, Buchner Labortechnik, Pfaffenhofen, Germany). The samples were stored at this temperature until use (maximum storage time: one week). Given the high concentration of maltodextrin as a stabiliser, the low storage temperature, and minimal temperature fluctuations ensured by the two-door freezer system, a short storage duration of up to one week is not expected to influence the drying behaviour of the sample (Flores and Goff, 1999; Smith et al., 2014). Additional details about the preparation process can be found in Kalinke and Kulozik (2023, 2024).

2.1.2. Dielectric properties and penetration depth

The dielectric properties, specifically the relative dielectric constant (ε') and the relative dielectric loss factor (ε''), were measured for 2450 ± 50 MHz using the μWaveAnalyser (Püschner, Schwanewede, Germany).

Temperature-dependent dielectric properties were investigated in duplicate for two distinct product states: fresh, frozen and fully-dried. The fresh, frozen foam samples were prepared as described above (Section 2.1.1) and measured within a temperature range of −20 °C to 0 °C. The fully microwave-freeze-dried samples were prepared as described in section 2.1.4 (MWFD at 220 W constant power supply, drying until mass constancy for 10 min). The dielectric properties of the fully-dried sample were measured within a temperature range of +10 °C to +75 °C. These ranges reflect the relevant temperature conditions of both product states encountered during MWFD.

The measurement protocol and setup for temperature-dependent dielectric property analysis followed the methodology and equipment configuration described in detail in Sickert et al. (2023b). In short, the samples and the measuring head were pre-tempered to the respective starting temperature of the measurement. The sample was placed in the measurement equipment and equilibrated at starting temperature for 1 h. Subsequently, the temperature was increased at 0.1 K/min using an external tempering system (Unistat 161 W, Huber, Offenburg, Germany). Temperature-dependent dielectric properties were recorded every 30 s using μWaveAnalyser 3.2.0 software (Püschner, Schwanewede, Germany). The temperature was recorded via a temperature sensor inserted into the measurement head using SpyControl 2.0 software (both from Huber, Offenburg, Germany). An empty vial measurement served as reference. The measurement data was processed using Matlab R2023a (MathWorks, Natick, MA, USA). The closed vial setup ensured stable water content throughout the measurement of each sample.

Dielectric properties characterise how a material interacts with an electromagnetic field. The dielectric constant ε' indicates the material's ability to store electrical energy, whereas the dielectric loss factor ε'' quantifies its ability to convert electromagnetic energy into heat. As a lossy material interacts with a microwave field, the electric field attenuates with increasing depth of propagation. This attenuation is described by the power dissipation penetration depth (d_p), which defines the depth at which the incident microwave power is reduced to 36.8 % (i.e., 1/e) of its original value. This concept assumes a plane wave propagating through a semi-infinite medium, where an exponential decay of the electric field occurs. This power dissipation penetration depth d_p can be calculated using Equation 1. (Datta and Anantheswaran, 2001)

$$d_p = \frac{\lambda_0}{2\pi\sqrt{2\varepsilon'}} * \left[\sqrt{1+\left(\frac{\varepsilon''}{\varepsilon'}\right)^2} - 1\right]^{-\frac{1}{2}} \quad (1)$$

Where λ_0 is the wavelength of the microwave in vacuum, for 2450 MHz i.e. 12.24 cm.

2.1.3. Dryer

The pilot-scale microwave freeze dryer (Model μVac0150fd) was connected to a computer and controlled using the associated process control software (μWaveCAT software), both supplied by Püschner Microwave Power Systems (Schwanewede, Germany). Data acquisition was realised during the process, capturing measurements every second for parameters including amongst others: sample weight, weight loss, product temperature, current microwave input power, and current microwave reflected power. These were recorded using a balance (Soemer, Lennestadt, Germany; accuracy ±0.01 g), an infrared pyrometer for temperature measurement (CT13.10, Heitronics, Wiesbaden, Germany), a magnetron microwave generator (MB2340A-140BW, Muegge, Reichelsheim, Germany), and a microwave reflection detector (μWRefAmp1.3 000337, integrated into the microwave freeze dryer). The magnetron microwave output power could be controlled continuously between 1000 W and 80 W via anode current/anode voltage adjustment. More common, so-called cycling of the magnetron for power modulation was not employed, as it is problematic in MWFD due to occurring power peaks resulting easily in undesirable plasma formation and subsequent, forced shutdown of the plant. The pyrometer's emissivity was pre-set by the drying plant manufacturer to suit the specific requirements of food material MWFD. Emissivity varies throughout the drying process (Ferrão et al., 2017). However, continuous emissivity adjustment during drying was not feasible. Consequently, a fixed emissivity setting was used. This was particularly suitable for measuring the temperature of the dried product surface under MWFD conditions.

As shown in Fig. 1, the freeze dryer comprised a two-chamber system: a cylindrical microwave chamber and a connected secondary chamber, housing the ice condenser (operated at −50 °C). The microwave chamber was equipped with a rotating turntable for sample movement (1.5 revolutions per minute). The turntable was connected to the balance for inline weight measurement. The microwave port connected the microwave chamber to a magnetron microwave generator (MB2340A-140BW, Muegge, Reichelsheim, Germany) operated at a nominal frequency of 2450 MHz, with a maximum output power of 1000 W and a minimum output power of 80 W (hardware limitation set by the plant manufacturer). The microwave chamber was connected via the ice condenser chamber to the vacuum system, which consisted of two vacuum pumps (Hena 61, Pfeiffer Vacuum, Aβlar, Germany; Ruvac WA501, Leybold, Cologne, Germany).

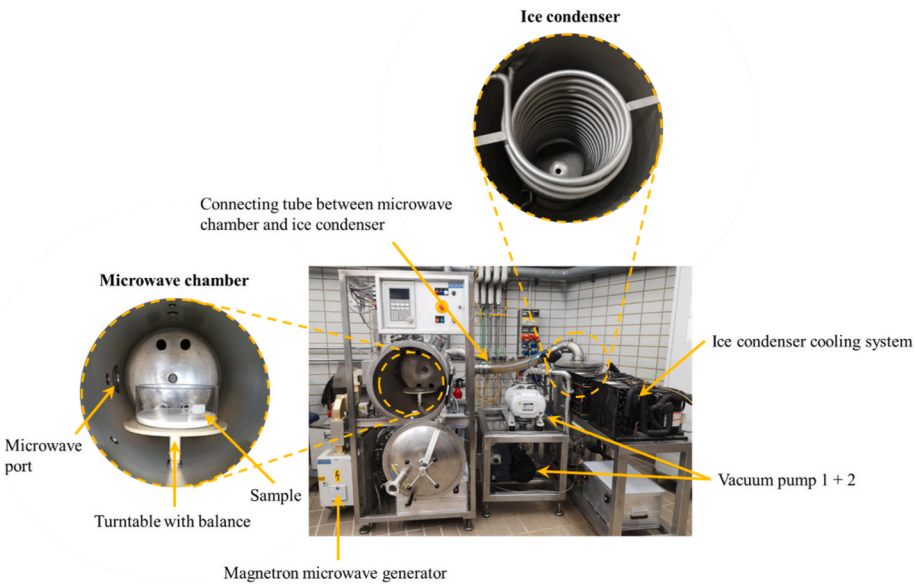


Fig. 1. Pilot-scale microwave freeze dryer featuring a two-chamber system: a microwave chamber (left) containing the sample placed on a rotating turntable, and an ice condenser chamber (top right) equipped with a cooling coil for the resublimation of generated water vapour. Additional details are provided through labels in the depiction.

2.1.4. Process settings

The pre-frozen maltodextrin foam sample was placed in the centre of the turntable of the pilot-scale microwave freeze-dryer system, and MWFD was conducted in duplicate under the settings specified in Table 1 and further elaborated in the following.

In this study, two process approaches were compared: the constant power approach and the adjusted power approach. The constant power approach represented the conventional MWFD process and served as the reference drying method. In this approach, a constant absolute microwave power was applied throughout the entire drying process. This constant power setting (P_{SET}) was investigated in the range of 120–220 W.

For the adjusted power approach, the absolute microwave input power was constantly readjusted to the current sample weight during drying. This adjustment was made every 1 s based on the measured current sample weight (m(t)). Different microwave power levels per gram of current sample weight were compared: 1, 2, 3, 3.2, 4, 5, and 6 W/g. Beside these set power levels (P_{SET}), Table 1 gives the resulting mean (forwarded) microwave power input ($\overline{P}$) during drying. Reasons for the small deviation between P_{SET} and $\overline{P}$ in the constant approach will be elucidated in the Results and Discussion section.

$\overline{P}$ was calculated as given in Equation (2):

$$\overline{P} = \frac{\sum_{t=0}^{t=t_{end}} (P_{FWD}(t) * \Delta t)}{t_{end}} \quad (2)$$

Where $P_{FWD}(t)$ is the current forwarded microwave input power in watts (W), t is the current drying time in seconds, starting from the application of the MWFD vacuum at t = 0 s —marking the onset of water removal, i.e. starting point of drying— and ending with t_{end}, which is the total drying duration in seconds. This drying duration is the time between the application of the vacuum and the attainment of a moisture ratio (MR) of 0.005 [-], as derived from literature (Ambros et al., 2016; Kalinke et al.,

Table 1
Specifications of the investigated MWFD process settings, showing the set microwave power levels for both, constant and adjusted power approach. For all settings, the resulting mean absolute microwave power input during drying was given. Power settings of both approaches sharing the same font colour resulted in the same mean microwave power input, as indicated by the same superscripted letters (ANOVA with post-hoc Bonferroni tests). * A minimum absolute power of 80 W had to be maintained. ** Only one successful repetition was possible.

Process constants	Power approach	Set microwave power (P_{SET})	Resulting mean absolute microwave power input ($\overline{P}$)	
Pressure setting: 0.1 mbar Turntable rotation speed: 1.5 rpm	constant	120 W	117.1 ±0.7 W^{I}	
		140 W	131.9 ±0.2 W^{H}	
		160 W	151.0 ±1.9 W^{G}	
		180 W	174.3 ±0.0 W^{F}	
		200 W	189.1 ±0.5 W^{E}	
		220 W	207.6 ±0.3 W^{D}	
	adjusted	1 W/g x m(t)	85.3 ±0.6 W^{J}	*
		2 W/g x m(t)	129.8 ±1.3 W^{H}	
		3 W/g x m(t)	190.8 ±2.4 W^{E}	
		3.2 W/g x m(t)	203.6 ±1.3 W^{D}	
		4 W/g x m(t)	245.9 ±4.8 W^{C}	
		5 W/g x m(t)	298.6 ±2.7 W^{B}	
		6 W/g x m(t)	346.4 W^{A}	**

2024; Kubbutat et al., 2020). The definition of this drying duration or so-called drying time is further detailed in the corresponding section below (Section 2.2.2). The time interval for which $P_{FWD}(t)$ was detected is 1 s, referred to as Δt.

Consequently, $\overline{P}$ indicates the average constant microwave power over the entire drying duration with which the individual power setting is to be equated with. More precisely, Table 1 highlights specific settings in the same font colours, i.e., 140 W and 2 W/g, 200 W and 3 W/g, and 220 W and 3.2 W/g. For these power settings of the two approaches, MWFD resulted statistically in the same $\overline{P}$. The 3.2 W/g adjusted microwave power setting was specifically selected for investigation because it not only matched the mean microwave power input $\overline{P}$ of MWFD at a constant power input of 220 W but also had the same drying duration. This allowed for a direct comparison between the two power approaches at 220 W and 3.2 W/g. This relationship will be discussed in more detail in the Results and Discussion section (Section 3.2).

Further, Table 1 marks the 1 W/g drying process with an asterisk (*), indicating that this drying process was affected by the system's minimum absolute microwave power of 80 W, which at the end of drying did not correspond to 1 W/g final sample weight. In this particular case, power was kept at 80 W as a minimum, because it was not possible to go below this power level due to hardware limitations. To highlight this particularity, all affected results in this study are marked with an asterisk (*), and the implications of this limitation are discussed accordingly. A double asterisk (**) is used in this study to indicate that the results of the 6 W/g drying process were based on only one successful trial. Further trials failed due to product overheating, as will be discussed in more detail in the Results and Discussion section.

MWFD was performed at a pressure of 0.1 mbar with simultaneous turntable rotation (1.5 rpm). The drying process was stopped when the sample weight remained constant for 10 consecutive minutes. The exact drying time was then calculated as described in Section 2.2.2.

2.2. Assessment of drying performance

2.2.1. Energy utilisation

The total microwave energy input (E_{TMEI}) was calculated according to Equation (3). It is the sum of all detected forwarded microwave input power values ($P_{FWD}(t)$) multiplied by their respective time intervals (Δt). $P_{FWD}(t)$ was detected by the integrated microwave generator system.

$$E_{TMEI} = \sum_{t=0}^{t=t_{end}} (P_{FWD}(t)*\Delta t) \tag{3}$$

Similarly, the reflected microwave energy input (E_{RFL}) was calculated according to Equation (4). It is the sum of all detected reflected microwave power values ($P_{RFL}(t)$) multiplied by their respective time intervals (Δt). $P_{RFL}(t)$ was detected by the integrated reflection detector.

$$E_{RFL} = \sum_{t=0}^{t=t_{end}} (P_{RFL}(t)*\Delta t) \tag{4}$$

The absorbed microwave energy (E_{ABS}) was calculated as the difference between E_{TMEI} and E_{RFL} (Equation (5)). It is common practice in literature that all energy that is not reflected back to the generator is considered absorbed by the sample. Even though, additional small losses in the waveguide, the cavity walls (Morgan, 1949), and the turntable made of polypropylene (PP) and polyether ether ketone (PEEK) (Zhang et al., 2006a) might occur, these small losses are commonly neglected (Ambros et al., 2016; Atuonwu and Tassou, 2018; Sickert et al., 2023b; Yang and Chen, 2024).

$$E_{ABS} = E_{TMEI} - E_{RFL} \tag{5}$$

Correspondingly, $P_{ABS}(t)$ indicates the currently absorbed portion of $P_{FWD}(t)$ that was not reflected back to the microwave generator ($P_{RFL}(t)$). As $P_{ABS}(t)$ cannot be directly measured, it is calculated using $P_{FWD}(t)$ and $P_{RFL}(t)$ as described in Equation (6).

$$P_{ABS}(t) = P_{FWD}(t) - P_{RFL}(t) \tag{6}$$

The proportion of absorbed microwave energy (PAE) indicates the energy efficiency of microwave application (Kalinke et al., 2023; Sickert et al., 2023b; Yang and Chen, 2024; Zhang et al., 2018). It is the ratio of absorbed microwave energy (E_{ABS}) to the total applied microwave energy (E_{TMEI}), as denoted in Equation (7).

$$PAE = \frac{E_{ABS}}{E_{TMEI}} \tag{7}$$

2.2.2. Drying speed

MWFD was assessed based on drying time, which was the duration between the application of vacuum and the attainment of a moisture ratio (MR) of 0.005 [-], as derived from literature (Ambros et al., 2016; Kubbutat et al., 2021). The MR was calculated using Equation (8):

$$MR(t) = \frac{m(t) - m_e}{m_0 - m_e} \tag{8}$$

Here, m(t) represents the sample mass at time t in gram, m_e is the equilibrium mass of the product in gram, and m_0 is the initial product mass at the onset of drying in gram. MR describes the normalised moisture content of a product during drying.

The negative derivative of MR(t) with respect to time was denoted as the drying rate, indicating the rate of MR reduction over the drying period.

2.2.3. Product temperature and temperature uniformity

The progression of product surface temperature was monitored using the integrated pyrometer of the drying plant. During each rotation of the turntable, and hence the sample, the pyrometer traced a circular measurement path on the sample surface. This circular path had a radius of 4 cm around the rotation axis of the sample. The temperature measurement spot of the pyrometer had a diameter of 2.5 cm. Consequently, the temperature data presented in this study represent the time-resolved temperature readings along this circular trajectory on the sample surface, rather than the average temperature of the entire sample.

Since the pyrometer's temperature measurement describes a circular path on the sample during each rotation, the formation of an inhomogeneous surface temperature pattern along this path results in temperature variations in the temperature readings. This can be related to the inhomogeneity of temperature distribution of the entire sample as cross-validated with independent measurement techniques. These include thermographic imaging, spatial colour change of thermochromic ink added to the product, and spatially resolved detection of residual enzyme activity in the product. The corresponding cross-validation data are presented in Kalinke and Kulozik (2023, 2024), where emphasis was placed on method development and validation. For this reason, detailed discussion of these aspects is omitted here. The cross-validation was conducted using the same processing plant, measurement setup, and equivalent sample design, thereby ensuring consistency and comparability of results. However, it is important to note that these earlier studies investigated temperature inhomogeneity under temperature-controlled (constant power) drying approaches, differing from the MWFD approaches investigated in the present study.

Temperature inhomogeneity during MWFD was quantified as the temperature difference between the coldest and hottest temperature detected along the circular measurement path on the sample. This temperature difference is referred to as the temperature oscillation span. The maximum temperature oscillation span observed throughout the entire MWFD process is termed the maximum temperature inhomogeneity.

2.2.4. Statistical analysis

Drying experiments were conducted at least in duplicate, and all reported errors refer to the average error of the replicates. Statistical significance of group differences was evaluated by analysis of variance (ANOVA) followed by post-hoc Bonferroni tests.

To test for significant differences between two mean values or between a mean value and a specific given value, t-tests were employed.

All differences were considered significant at $p < 0.05$. Statistical analysis was performed using OriginPro 2023 software (OriginLab Corp., Northampton, MA, USA).

3. Results and discussion

3.1. Dielectric properties

The dielectric properties of the sample are presented in Fig. 2, covering both the initial (fresh and frozen) and final (fully-dried) product states, along with the respective temperature ranges relevant to each condition.

For the fresh, frozen state, dielectric measurements were conducted within a temperature range of −20 °C to 0 °C. Due to the high water content and foamed structure, the fresh samples lacked structural stability when not frozen, making measurements above 0 °C in a fresh, unfrozen state faulty. Additionally, temperatures above 0 °C are only reached in the desorption drying stage of freeze-drying, by which point the freezable, free water has already been removed from the sample. Consequently, the fresh, water-rich sample does not exist in a non-frozen state during MWFD. More precisely, the dielectric properties at −20 °C are considered most representative of the sample at the onset of drying, as this temperature best aligns with the sublimation temperature of pure water at the operating pressure of 0.1 mbar, i.e. −42 °C (Marti and Mauersberger, 1993). Measurements at temperatures below −20 °C were not feasible due to hardware limitations.

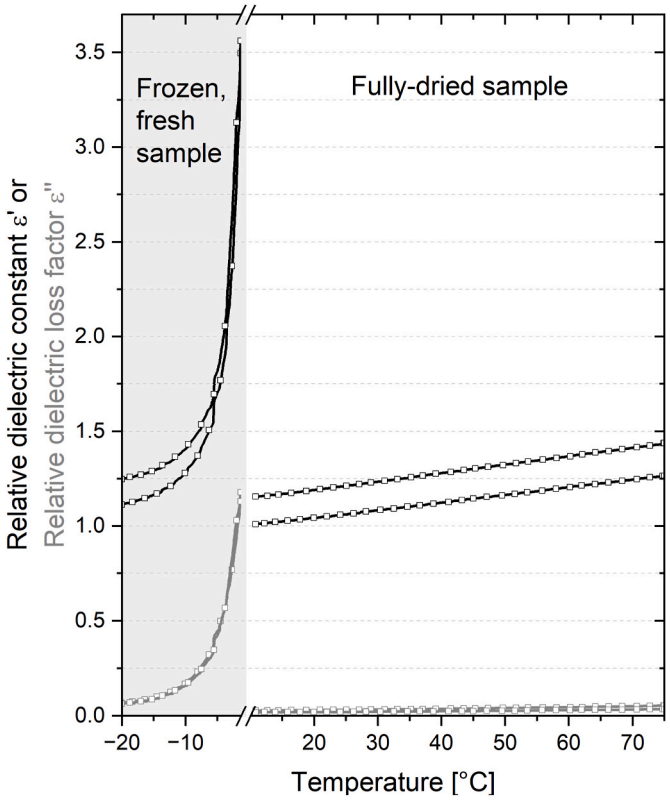


Fig. 2. Relative dielectric constant ε' (black) and relative dielectric loss factor ε'' (grey) for the frozen, fresh sample (left) and the fully-dried sample (right) in response to sample temperature. Results are given for two individual specimen per sample state. For better readability of the data, symbols were only given for every 50th data point.

For the fully dried state, measurements were performed between +10 °C and +75 °C. Due to hardware constraints, measurements above +75 °C could not be conducted. The final product temperature at the end of MWFD varied strongly depending on the applied microwave power, as discussed later in Section 3.3.3. However, it is reasonable to assume that the dielectric properties measured at the highest feasible temperature of +75 °C best represent the end-of-drying temperature condition in the context of this study.

Based on these temperature settings, the fresh, frozen state is best described by $\varepsilon' = 1.180 \pm 0.067$ and $\varepsilon'' = 0.066 \pm 0.002$ (at −20 °C). The fully-dried state can be approximated with $\varepsilon' = 1.351 \pm 0.087$ and $\varepsilon'' = 0.045 \pm 0.010$ (at +75 °C). For comparison, fresh, water-rich foods that are neither dried nor frozen, typically exhibit ε' values between 40 and 60 and ε'' ranging from 10 to 20 (Datta and Anantheswaran, 2001; Regier et al., 2017). For frozen vegetable products (peas, carrots, potatoes) at −20 °C, ε' was reported to be between 4.1 and 4.6 and ε'' between 0.29 and 0.32 (Bengtsson and Risman, 1971). Due to low water content and high porosity, the dielectric properties of freeze-dried products are especially low. Sickert et al. (2023b) reported $\varepsilon' = 1.26$ and $\varepsilon'' = 0.05$ for freeze-dried Tylose gel at 20 °C. Highly porous materials, such as foam samples, exhibit even more reduced dielectric properties after freeze-drying due to the increased volume fraction of air, as seen here.

Based on the measured dielectric data in this study, the power dissipation penetration depth was calculated as 32 cm in the frozen state and 50 cm in the fully-dried state. For comparison, frozen vegetable products are at 13–14 cm, freeze-dried Tylose gel at 44 cm. This range indicates that a limitation by penetration depth is not the main cause of temperature inhomogeneities observed in this study and probably, most MWFD food processes. Sample dimensions and dielectric properties are within a range where resonance effects and deviations from exponential field decay can occur in the sample (Datta and Anantheswaran, 2001). This is important, as penetration depths in non-frozen, water-rich food matrices are typically only 1–2 cm, playing a significant role in the formation of heating patterns inside non-frozen, non-dried food matrixes (Datta and Anantheswaran, 2001).

Given the small range of variations of dielectric properties of our sample during MWFD, consistent with findings reported in Sickert et al. (2023b) for MWFD of Tylose gel, a detailed discussion of the temperature-dependence and specific dielectric property values is omitted.

Importantly, no macroscopic structural changes were observed in any of the MWFD trials presented in this study. This is important, as increasing temperatures within the frozen state can lead to an increasing fraction of liquid, free water in the sample, which leads to a vast increase in dielectric properties, as can be seen in Fig. 2 and is in line with literature (Datta and Anantheswaran, 2001). This would trigger melting of ice in MWFD leading to a thermal runaway, where localised melting occurs and accelerates further heating and structural collapse of the sample. In this study, however, no such effects were observed.

3.2. Direct comparison of drying approaches

The two approaches of microwave power input (constant and adjusted) were compared in terms of differences of microwave input, temperature progression, and drying rate over drying time. Therefore, Figs. 3–5 compare the progression of current microwave power (Fig. 3), product temperature (Fig. 4), and the corresponding drying rates (Fig. 5) of a 220 W constant power approach compared to a 3.2 W/g adjusted power approach. These power settings (220 W and 3.2 W/g) were selected as they resulted in the same mean microwave power input and drying duration for both approaches, as will be discussed in the following. It is to be noted that selected data representing the constant power approach were adapted from Kalinke et al. (2024). Such data is

clearly indicated in the captions of each figure. These data serve exclusively as a reference for comparison with the adjusted power approach under identical product and process conditions. The constant power approach represents the current state-of-the-art MWFD in this context, while the adjusted approach is evaluated directly against this established approach using fully original experimental data in this study.

3.2.1. Microwave power

Fig. 3 gives the progression of microwave input power $P_{FWD}(t)$ for both approaches, represented by the continuous lines in the graph. Both approaches exhibited a power peak at maximum magnetron input power after approximately 5 min of drying. Nevertheless, the beginning of drying time started at 0 min, the moment the vacuum was applied and water removal from the sample started. The power peak at 5 min occurred once vacuum conditions were established in the drying chamber and the magnetron microwave generator was initially switched on. This initial switch-on power peak is typical for magnetron microwave systems (van der Merwe and Swardt, 2017).

In the adjusted power approach (grey), the microwave input was highest at the beginning of the process and gradually decreased to a minimum – from approximately 386 W to a minimum of 144 W at the end of drying. This resulted in an average microwave input power $\overline{P}$ of 203.6 W for the 3.2 W/g adjusted power approach. In the constant power approach, $\overline{P}$ was 207.6 W. The slight deviation of 207.6 W from the set value of 220 W occurred mainly because there was no microwave input during the first 5 min of drying. Most importantly, both depicted drying processes in Fig. 3 resulted in comparable $\overline{P}$ over the entire drying process (Table 1, Material and Methods section). Due to similar drying times, the total microwave energy input E_{TMEI} was also approximately the same in this specific case. This relationship is not universally valid, as will be discussed later in this study (Section 3.3.1). Moreover, this alignment was the reason why the selected power settings were chosen for the direct comparison of the two approaches in this section (Section 3.2), as it allowed for a clearer understanding of the differences between both approaches.

Further, Fig. 3 shows the progression of absorbed microwave power $P_{ABS}(t)$ as non-connected data points in the graph. For clarity, only every 120th data point (representing 2-min intervals) was displayed. The depiction demonstrates that $P_{ABS}(t)$ closely follows the progression of $P_{FWD}(t)$. Additionally, from the adjusted approach data (grey) it can be observed, that the relative proportion of input power absorbed by the sample increased slightly with decreasing input power. This effect has been previously documented for constant power application in magnetron microwave generators in literature (Taghian Dinani et al., 2020). It is important to note that the portion of microwave energy absorption is highly dependent on various product and equipment-specific factors (Sickert et al., 2023b; Wang et al., 2015; Yang and Chen, 2022; Zhang and Datta, 2003; Zhou et al., 2023). On average, both approaches demonstrated a comparable mean proportion of absorbed energy (PAE) along drying: PAE of 88 % for the constant approach versus 92 % for the adjusted approach. These values are high and consequently, beneficial for efficient microwave absorption. They are consistent with reported PAE values achieved for frozen mashed potato (Yang and Chen, 2022) and in line with values for different frequency settings in MWFD of Tylose gel (Kaysan et al., 2024). They can be attributed to a preliminary, one-time impedance matching performed prior to the start of all drying trials presented in this study using an integrated manual phase tuner, as described in Schmidt et al. (2022). Such load matching was essential to ensure safe operation of the MWFD system under low-load conditions typical for MWFD and to prevent potential equipment damage and corona discharge.

The observed differences in $P_{ABS}(t)$ were primarily attributable to variations in $P_{FWD}(t)$ rather than differences in the PAE value. Consequently, the discussion later in this section focuses only on changes in $P_{FWD}(t)$.

3.2.2. Product temperature

Fig. 4 depicts the temperature progression resulting from the two microwave power approaches.

Oscillations in the temperature data resulted from measurements taken outside the sample's rotation axis during simultaneous turntable rotation. These oscillations reflect the surface temperature variations along a circular measurement path on the sample, as detailed in Section 2.2.3. Preliminary studies have cross-validated that the extent of these oscillations provide a reliable indication of overall temperature inhomogeneity of the sample during temperature-controlled MWFD in the same MWFD plant (Kalinke et al., 2024; Kalinke and Kulozik, 2024).

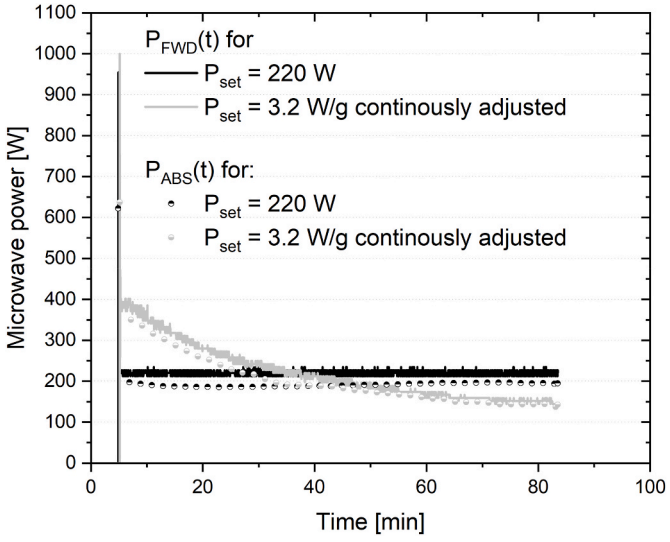


Fig. 3. Microwave input power $P_{FWD}(t)$ and absorbed microwave power $P_{ABS}(t)$ along drying; Results were given for the constant (black) and adjusted (grey) microwave power approach at 220 W and 3.2 W/g, respectively; For better readability, only the course of one exemplary drying process per approach was given. For the absorbed microwave power, only every 120th data point was given.

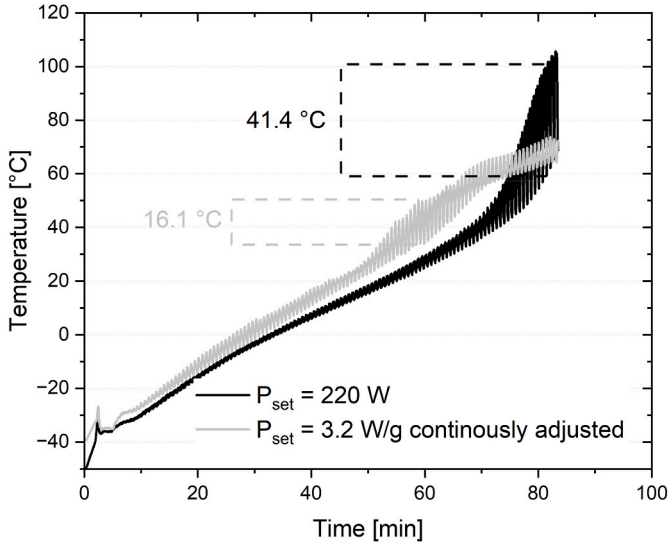


Fig. 4. Temperature progression along drying for the constant power approach (220 W) and the adjusted power approach (3.2 W/g), represented by black and grey lines, respectively. For clarity, only one temperature curve is shown for each approach. Brackets highlight the time and extent of the maximum temperature oscillation span, with the corresponding temperature disparity indicated.

This was validated by comparing temperature oscillation spans with results from other spatially resolved temperature measurement techniques, i.e. thermographic images, spatially-resolved thermochromic ink coloration and biomarker inactivation, as reported in both studies.

Fig. 4 shows that, at the beginning of drying, the adjusted power approach led to slightly higher product temperatures compared to the constant power approach. However, the temperature progression during the first half of the drying process was largely similar for both approaches. Towards the end of drying, the product temperature in the constant power approach surpassed that of the adjusted power approach, leading to higher final product temperatures in the constant approach. Specifically, the constant approach yielded a final mean product temperature of 85.5 °C, while the adjusted approach reached only 68.9 °C. The difference became even more pronounced when comparing the maximum final product temperatures at the hottest detected hotspot positions (i.e. maximum temperature of the temperature curve): 105.7 °C for the constant power approach versus 72.8 °C for the adjusted power approach.

These differences can directly be linked to the varying microwave power levels at each point in time (see Fig. 3). The slightly higher product temperature at the beginning of drying can be attributed to a higher initial power input in the adjusted approach. This resulted in greater heat transfer to the sample in the beginning of this approach. It should be emphasised that the product temperatures were measured on the sample's surface. During freeze-drying, the sublimation front gradually moves inward. As a result, the detected surface temperature does not represent the sublimation temperature but exceeds it in the already-dried surface layer – already so, during the sublimation drying phase (Jiang et al., 2022; Khalloufi et al., 2005).

Likewise, higher final product temperatures in the constant power approach resulted from higher final microwave power input. The temperature difference between the two approaches is more pronounced at the end of drying due to exponentially increasing product temperatures. In desorption drying, since most water is removed during sublimation, less heat is needed for evaporation, allowing more heat to raise the product's temperature, leading to a significant increase in product temperature at the end of MWFD (Duan et al., 2012). In the adjusted power approach, microwave power levels and consequently, heat transfer to the sample were low during the final drying stage. This explains why for the adjusted approach, the exponential temperature rise was less pronounced and eventually levelled off, as the microwave power input and corresponding heat transfer were gradually reduced along drying. This was in-line with findings from Duan et al. (2012) on preventing product overheating by step-wise power reduction in MWFD.

3.2.3. *Temperature uniformity*

In addition to the overall progression of product temperatures, Fig. 4 also highlights differences in temperature oscillation span between the constant and adjusted power approaches. At the beginning of the drying, the adjusted approach exhibited a slightly higher temperature oscillation span than the constant approach. However, this trend reversed towards the end of drying. For the adjusted approach, temperature inhomogeneity peaked at 59 min and then steadily decreased again. In contrast, temperature inhomogeneity in the constant approach began to increase, starting at 70 min, and continued to increase and stay high until the end of drying. Overall, the maximum temperature oscillation span for the constant power approach was 41.4 °C (at 81 min), substantially higher than the 16.1 °C observed in the adjusted power approach (at 59 min). These maximum temperature oscillation spans are highlighted within Fig. 4.

The described differences in temperature inhomogeneity between both approaches can be explained by two overlaying effects: 1) Temperature inhomogeneity is known to increase with increasing microwave power levels. 2) Temperature inhomogeneity is reported to increase towards the end of drying, especially during the transition between sublimation and desorption drying. Both effects are elucidated in more detail in the following:

Effect 1), Increasing inhomogeneity with increasing microwave power: This effect is attributed to the potential of greater regional disparities in microwave field strength with increasing microwave power levels. Additionally, higher microwave input power levels also result in shorter drying times (Abbasi and Azari, 2009; Ambros et al., 2018; Duan et al., 2010; Kalinke et al., 2024; Ozcelik et al., 2019a; Ozkan et al., 2007; Wang et al., 2009; Wang and Xi, 2005). This gives temperature inhomogeneities inside the product less time to equilibrate via conductive heat transfer. In a longer drying process, there is more time available for this equilibration effect. In brief, decreasing microwave input power leads to slower drying and yields in higher temperature uniformity. This equilibration effect is better known from intermittent microwave application, where microwave input is actively turned on and off to increase temperature equilibration times (Oliveira and Franca, 2002; Yang and Gunasekaran, 2001, 2004). For intermittent microwave application the activation ratio of microwave input is decreased to prolong equilibration times.

Effect 2), temperature inhomogeneity in MWFD increases towards the end of drying. This is based on previous studies (Jiang et al., 2013b; Kalinke et al., 2024; Kalinke and Kulozik, 2024), reporting an increase in temperature inhomogeneity during the transition from sublimation to desorption drying for constant microwave power input. Jiang et al. (2013b) investigated MWFD of banana chips and proposed that this phenomenon could be attributed to a thermal runaway effect, triggered by the localised melting of individual ice crystals within the sample. Liquid, free water has significantly higher dielectric properties (Kaatze and Uhlendorf, 1981) compared to frozen water (Mätzler and Wegmüller, 1987) or bound water in MWFD samples (Sickert et al., 2023b). Consequently, segments of the sample where ice begins to melt, experience a sharp increase in dielectric properties. This increases microwave energy absorption and exacerbates existing temperature disparities.

In our opinion, such localised ice melting in our structurally delicate foam samples would trigger a chain reaction, causing adjacent ice to melt as well. This process should manifest in macroscopic structural loss of the sample due to regional ice melting and the structural instability of foam in a melted stage. However, this did not apply for our samples, as no structural loss was observed in this study, despite high reported levels of temperature inhomogeneity (see Section 3.3.3). Consequently, we believe the following explanation for effect 2) is likely: Temperature inhomogeneity becomes more pronounced during the transition from sublimation drying to desorption drying due to the differing drying behaviours across the sample. During this transition phase, hot spot regions of the sample enter the slower desorption drying stage, where temperature rises exponentially. Meanwhile, cold spots with higher water content remain in the faster sublimation drying stage, characterised by more gradual temperature increases.

These differences in drying stages affect how heat is distributed and utilised across the sample. In the cold spots, much of the available heat is consumed as latent heat to convert ice into vapour, producing a strong cooling effect resulting from a faster drying rate due to a still higher water content in these cold spot regions. In contrast, the hot spots in the desorption drying stage experience reduced cooling due to lower drying rates, while still being exposed to higher levels of microwave energy. This causes rapid temperature increases in the hot spots while cold spot temperature lags behind. As a result, the temperature disparities between the hot and cold spots grow during this transition phase, driven by the varying drying progress and consequently, heat utilisation across the sample. This interpretation is derived from previous findings on MWFD using a (temperature-controlled) constant microwave power approach (Kalinke et al., 2024; Kalinke and Kulozik, 2024).

Our previous study has shown that for the specific sample type and geometry used, the microwave-induced inhomogeneous heating pattern during MWFD predominantly develops in the horizontal direction (Kalinke and Kulozik, 2023). So even though, the surface temperature

was measured, this temperature is significantly affected by the presence or absence of a cooling effect in the underlying sample regions.

A combination of the aforementioned effect 1) and 2) helps to explain the observed different progression of temperature inhomogeneity between the novel adjusted and established constant power approach:

For the adjusted power approach, temperature inhomogeneity was only slightly higher at the start of drying compared to the constant power approach, peaking early before decreasing toward the end of the process. Generally, high microwave power caused greater temperature inhomogeneity (effect 1). However, in this case, the higher power levels were applied at the beginning of drying, a stage that is less prone to temperature inhomogeneity (effect 2). During the transition phase, as expected, inhomogeneity increased (effect 2). Shortly after, it declined again because microwave power was gradually reduced (effect 1), even though this phase is typically more susceptible to temperature inhomogeneity. However, the impact of microwave power reduction prevailed. Given the central role of the temperature profile shown in Fig. 4, its reproducibility was verified through two additional trials, both of which demonstrated the same temperature inhomogeneity behaviour as described here.

The progression of temperature inhomogeneity of our novel adjusted approach was similar to previous findings for temperature-controlled constant-power approaches (Kalinke et al., 2024; Kalinke and Kulozik, 2023, 2024), where microwave power was applied in a pulsed mode at the end of drying to prevent exceeding of a pre-set maximum temperature level. In this case, constant microwave power was nominally reduced, but only near the end of drying to maintain the product temperature at the specified maximum level. Similarly, temperature inhomogeneity initially increased as drying progressed but declined following the reduction in microwave power due to pulsed power application.

Further, the earlier onset of increasing inhomogeneity in the adjusted power approach—at approximately 50 min compared to 70 min in the constant power approach—can be attributed to its higher initial power input. This higher initial power led to a more advanced drying state for the adjusted approach at 50 min compared to the constant approach. As a result, the transition phase between sublimation and desorption drying was reached earlier in time for the adjusted approach, causing temperature inhomogeneity to appear sooner.

In contrast, for the constant power approach, temperature inhomogeneity increased throughout the drying process, as expected from effect 2. The absolute microwave power level remained consistently high (no effect 1), including the inhomogeneity-prone transition phase and up to the end of drying. This resulted in a progression of temperature inhomogeneity, as previously reported for constant microwave power input in MWFD (Jiang et al., 2013b; Kalinke et al., 2024; Kalinke and Kulozik, 2024). A more detailed discussion of the constant approach is omitted here, as constant approach data primarily serves as a reference to support the comparability of novel findings obtained with the adjusted power approach.

3.2.4. Drying rate

In general, Fig. 5 shows that with progressing drying, the drying rate decreases due to higher mass transfer resistance and lower levels of free water in the sample in both adjusted (grey) and constant (black) approach. Further, an initially faster drying in the adjusted approach compared to the constant approach can be seen.

The adjusted power approach achieved higher drying rates during the first 30 min of drying compared to the constant approach. However, after the 30-min mark, the constant power approach surpassed it in drying rate. This shift roughly coincided with the point in time when the microwave input power in the adjusted approach dropped below that of the constant approach, occurring at approximately 38 min into the drying process (see Fig. 3). This was expected and in line with literature (Ambros et al., 2018) as for a heat transfer-limited MWFD process,

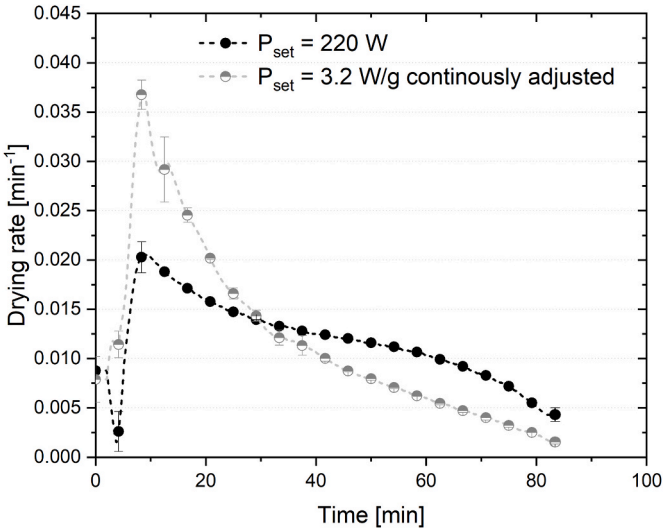


Fig. 5. Drying rate progression over time for the constant power approach (220 W; Data from Kalinke et al. (2024)) and the adjusted power approach (3.2 W/g; Data from this study), represented by black and grey symbols, respectively.

higher absolute microwave power input results in higher drying rates. Interestingly, the drying rate of the adjusted approach began to fall below that of the constant approach slightly before the 38-min mark, despite the microwave power input in the adjusted approach being still equal to that of the constant approach. This can be explained by the more advanced drying state of the adjusted approach at that point.

Overall, Fig. 5 demonstrates that for the adjusted approach the higher drying rates achieved at the beginning of the drying process fully compensated for the lower drying rates observed towards the end. This resulted in an equally fast drying process for both approaches. However, in the adjusted approach this was achieved at additionally lower final product temperatures and reduced temperature inhomogeneity. This demonstrates that the adjusted approach positively affected the temperature development of the sample, without resulting in a trade-off in drying time, as hypothesised. This was in line with findings on drying time and prevention of product overheating by step-wise power reduction reported for MWFD of apple slices in Duan et al. (2012).

3.3. Comparison of approaches at all investigated power settings

In this section, both approaches were compared across all investigated power settings, extending beyond the specific scenario presented and discussed in Section 3.2. To represent the constant power approach, selected data adapted from Kalinke et al. (2024) were used as a reference. This was clearly indicated in the figure captions. These data serve solely as a basis for discussing differences between both approaches. A separate discussion of the constant power approach is intentionally omitted, as it is available in detail in the original publication. All data and discussion related to the adjusted approach is completely original.

3.3.1. Drying time

Fig. 6 depicts the drying times of the adjusted and constant microwave power approach for all investigated power settings. By plotting the drying times of both approaches against their mean actual microwave input power values $\overline{P}$, a fair comparison was ensured. For drying at a constant microwave power level, $\overline{P}$ closely matched the set levels P_{SET} (e.g., 120, 140, … 220 W). As discussed before, minor deviations occurred due to the first 5 min of drying without microwave input.

From the drying times in Fig. 6, three main results can be derived and are discussed in the following.

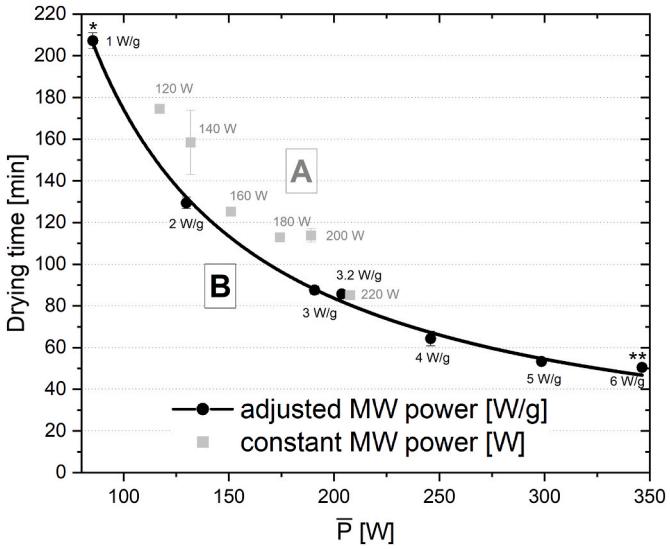


Fig. 6. Drying times resulting from the adjusted power approach (black, Data from this study) and the constant power approach (grey; Drying time data adapted from Kalinke et al. (2024)) for different settings of microwave input power, as indicated next to each data point. Drying times are plotted against the mean microwave power input throughout the drying process $\overline{P}$. For the adjusted approach, an interpolation curve is given for better comparability of both approaches. * Minimum absolute power of 80 W had to be maintained. ** Only one successful repetition was possible. **A** and **B** indicate that on average drying with the adjusted approach was significantly faster than drying with the constant approach.

1) for the adjusted power approach, MWFD could be conducted at higher levels of $\overline{P}$ than for the constant power approach. For the adjusted power approach, a $\overline{P}$ of 346.4 W could be realised, for the constant power approach only 207.6 W was feasible. These lower levels of microwave power input in the constant approach, already resulted in excessively high sample temperatures at the end of drying. This caused a forced shutdown of the drying process to prevent equipment damage, making it impossible to investigate higher power levels.

In the adjusted approach, a higher $\overline{P}$ was possible because high microwave power levels were applied at the beginning of the drying process (Fig. 3). At this stage, the intense heat transfer did not yet cause a significant temperature increase in the sample (Fig. 4) but effectively supported a high sublimation rate (Fig. 5). Toward the end of the drying process, however, the microwave input power was significantly lower than in the constant approach (Fig. 3). As a result, less heat was introduced during this phase, where the sample temperature increased exponentially (Fig. 4). Therefore, in the adjusted approach, the final product temperature did not rise as sharply as in the constant approach (Fig. 4). Consequently, the risk of a forced shutdown due to excessive overheating was reduced, even at the same average power $\overline{P}$. This was in line with findings from Duan et al. (2012). Moreover, they also reported that these lower final product temperatures were responsible for a better product quality after MWFD with a reducing power approach compared to a constant power approach.

2) For both approaches, higher $\overline{P}$ resulted in faster drying. However, in contrast to the constant approach, in the adjusted approach this did not result in a linear reduction of drying time but an asymptotic approximation to a minimum drying time. This asymptotic trend occurred because the adjusted approach allowed for a wider range of microwave power inputs to be investigated. Drying time cannot endlessly be reduced by increasing heat transfer. At sufficiently high power levels, sublimation drying is no longer constrained by heat but rather by mass transfer (Pikal, 1994). While the exact relationship between drying time and microwave power depends on the specific product, the initial linear trend (Ambros et al., 2018; Duan et al., 2010) and the asymptotic levelling off at higher power inputs (Wang et al., 2009) align with observations in other studies. Notably, the adjusted approach accelerated drying to the point where mass transfer limitations became apparent—something not achieved with the constant approach.
3) the adjusted approach resulted in significantly shorter drying times compared to drying at the same $\overline{P}$ in the constant approach (*t*-test, $p < 0.05$). On average, this reduction was 18.9 ± 9.4 min, equivalent to an averaged 14 % drying time reduction. This was derived from drying times reported for the constant approach compared with drying times at the same $\overline{P}$ estimated from the interpolated curve for the adjusted power approach (black curve given in Fig. 6, interpolation defined by: $y = a^*x^b$, $R^2 = 0.998$). Thereby, the time difference by which the adjusted approach was faster than the constant approach became smaller with increasing $\overline{P}$.

On average, the faster drying observed in the adjusted approach can be explained by the same principle as before: Higher heat transfer at the beginning of drying promoted a greater sublimation rate, compensating for reduced heat transfer at the end. Toward the end of drying, increased heat transfer only minimally contributes to higher desorption drying rates and, therefore, faster drying. In contrast, applying the same heat at the beginning of drying led to significantly greater drying rates than the same heat would have achieved at the end. As $\overline{P}$ increased, the benefit of faster drying with the adjusted approach decreased. This was because the maximum drying rate, which occurred at the start, became increasingly constrained by mass transfer limitations and could no longer rise with additional heat input. In summary, the adjusted approach optimised microwave energy utilisation by applying higher power at the start and reducing it at the end, making heat input more efficient for water removal and accelerated drying. The efficiency of microwave energy utilisation will be further discussed in Section 3.3.2.

3.3.2. Energy demand

3.3.2.1. Microwave energy demand. Fig. 7 depicts the total microwave energy input E_{TMEI} in dependence of $\overline{P}$ for both approaches.

From Fig. 7, two main outcomes can be derived and will be discussed in the following.

1) For both approaches, the E_{TMEI} was independent of $\overline{P}$. More precisely, no significant increasing or decreasing trend of data was observed (*t*-test, $p < 0.05$). At lower power levels, slower drying rates extended the drying duration, compensating for the reduced power input by a prolonged power application time. This balancing mechanism explains why E_{TMEI} remained consistent within each approach. This observation was expected and aligns with findings from previous studies for the established, constant power approaches in MWFD (Ambros et al., 2018; Kalinke et al., 2024).
2) E_{TMEI} was significantly lower for the adjusted approach than the constant power approach (*t*-test; $p < 0.05$). The adjusted approach reduced E_{TMEI} by 0.050 kWh, which corresponds to a 15 % decrease compared to the constant power approach. Different portions of absorption of E_{TMEI} between both approaches did not account for the observed differences, as described in more detail in section 3.2.1. The savings were the direct result of shorter drying times achieved at the same $\overline{P}$ (Fig. 6). This indicates that the adjusted approach utilised microwave energy more efficiently for drying, as previously mentioned. In our opinion, the key factor driving this improved efficiency was the timing of heat transfer during the drying process. In the adjusted approach, most heat transfer occurred during the

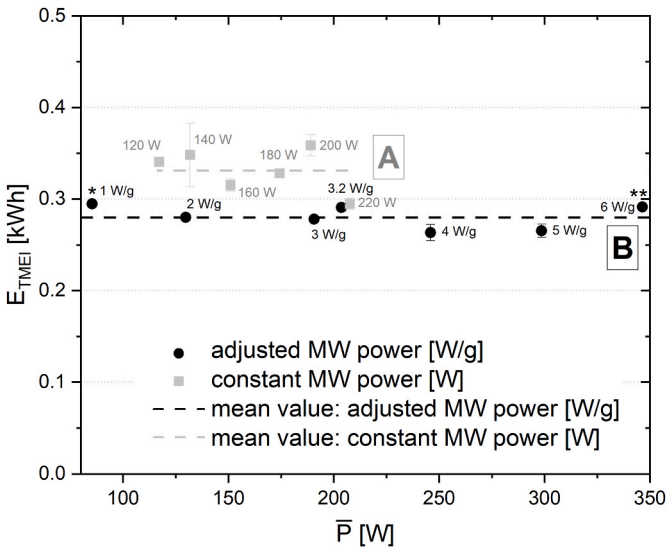


Fig. 7. Total microwave energy input E_{TMEI} along drying resulting from the adjusted power approach (black; Data from this study) and the constant power approach (grey, E_{TMEI} data adapted from Kalinke et al. (2024)) for different settings of microwave input power, as indicated next to each data point. Total microwave energy input was plotted against the mean microwave power input throughout the drying process $\overline{P}$. Horizontal lines indicate the mean value of all E_{TMEI} values of each approach. **A** and **B** indicate that on average drying with the adjusted approach resulted in a significantly lower E_{TMEI} than drying with the constant approach. * Minimum absolute power of 80 W had to be maintained. ** Only one successful repetition possible.

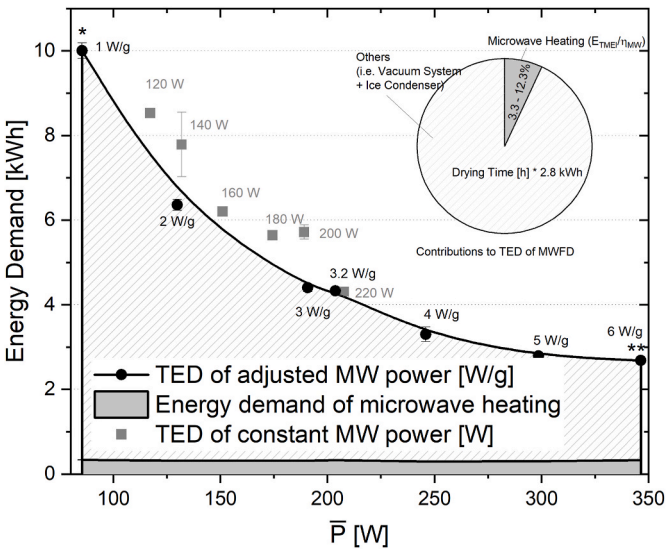


Fig. 8. Total energy demand (TED) of drying for the adjusted approach (black; Data from this study) and the constant approach (grey; TED data adapted from Kalinke et al. (2024)), the grey filled share of TED depicts the portion of TED of the adjusted approach resulting from microwave heating. Energy demand data was plotted against the mean microwave power input throughout the drying process $\overline{P}$. * Minimum absolute power of 80 W had to be maintained. ** Only one successful repetition possible.

beginning of the process when drying was primarily heat-transfer-limited. In heat-transfer-limited drying, the availability of heat is the bottleneck of drying rate. In this case, increasing heat transfer accelerates drying. In later stages of drying, drying becomes increasingly mass-transfer-limited due to an increasing mass transfer resistance (Pikal, 1994). Here, increasing heat transfer does not result in faster drying. The drying rate is limited by the maximum water vapour mass transfer that can be supported by the already dried product matrix. In our opinion, this explains why the adjusted approach effectively enhanced the utilisation of microwave energy input, as this approach concentrates a larger portion of total heat transfer in the heat-transfer-limited phase of drying.

3.3.2.2. Total energy demand. As known from literature (Ambros et al., 2018; Jiang et al., 2013a; Kalinke and Kulozik, 2024), the overall energy demand of MWFD is primarily governed by the drying time. The drying time determines the operational duration of the most energy-intensive components, such as the vacuum system and the ice condenser cooling unit. For the plant setup used in this study, energy demand can be calculated based on drying time, E_{TMEI}, magnetron efficiency (η_{MW} = 0.88) and the specific energy demand of the plant peripherals (2.8 kWh), as reported in Kalinke and Kulozik (2024) for temperature-controlled MWFD in the same drying equipment at 0.1 mbar. Applying this methodology, the energy demand for microwave heating accounted for approximately 3.3–12.3 % of the total energy consumption, as detailed in Fig. 8. In contrast, 87.7–96.7 % of the total energy demand was attributed to plant peripheral systems, their consumption scaled proportionally with drying time. Accordingly, the total energy demand presented in Fig. 8 closely mirrors the drying time trends shown in Fig. 6 (Section 3.3.1). To avoid redundancy, a detailed discussion of this data is omitted here.

In essence, the adjusted drying approach offers clear energy advantages over the constant approach by significantly reducing drying times. These reductions can be achieved either by enabling faster drying at equal $\overline{P}$ or by increasing $\overline{P}$ to accelerate drying. While the lower E_{TMEI} associated with the adjusted approach is also beneficial, the dominant factor influencing total energy demand remains the drying time. Of course, in an industrial scale, the energy demand reduction resulting from lower E_{TMEI} might play a more significant role than reported for our pilot-scale setup.

Overall, this shows that the adjusted approach is beneficial in regard to total energy demand as both, the energy demand for microwave heating (Section 3.3.2) and the run time of the equipment (Section 3.3.1) can be significantly reduced compared to the constant approach.

3.3.3. Temperature uniformity

Temperature inhomogeneity is a critical consideration in microwave processing, as it often trades off with time and energy efficiency. The goal of the adjusted approach was to alter microwave input power level continuously to achieve both, energy efficiency and uniformity. Fig. 9 compares the constant power approach and the adjusted power approach in terms of temperature progression during drying (right axis), given only for one representative repetition per setting for better readability. The moisture ratio, shown on the left axis, represents the normalised sample weight over time and is presented as the mean of all repetitions to highlight differences in drying behaviour across power settings. The inhomogeneity was evaluated based on temperature disparities during drying. The temperature oscillation span of the temperature curve was used as an indicator for these temperature disparities, a metric cross-validated for this purpose in earlier studies (Kalinke et al., 2024; Kalinke and Kulozik, 2023, 2024). A larger temperature oscillation span reflects higher temperature inhomogeneity of the process.

For better comparability, maximum temperature inhomogeneity for each setting were additionally given in Table 2.

The two main findings from Fig. 9 are discussed in the following.

1) For both approaches, temperature inhomogeneity increased with higher averaged microwave power levels (*t*-test; $p < 0.05$). This was expected, as it aligns with findings from previous studies for different levels of constant microwave power input in microwave drying (Kalinke et al., 2024; Oliveira and Franca, 2002; Ozcelik et al., 2019b; Yang and Gunasekaran, 2001, 2004). As described in Section

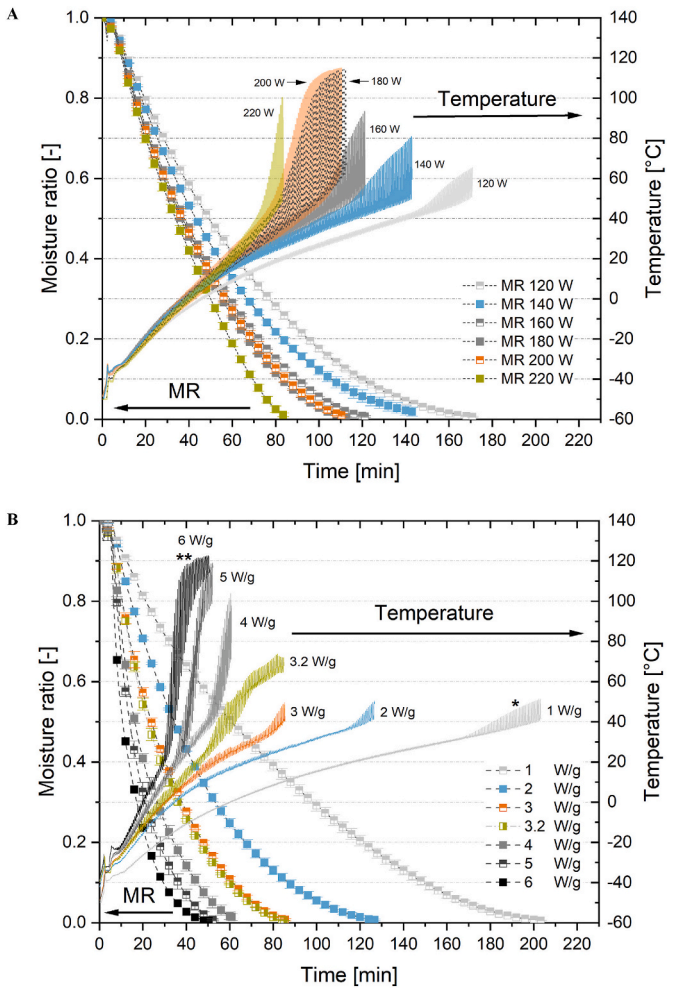


Fig. 9. Progression of temperature (right axis) and moisture ratio (MR, left axis) over drying time using the constant power approach (**Panel A**) and the adjusted power approach (**Panel B**). Individual curves represent different microwave input power settings, as specified in the legend and adjacent to the curve. Colours (blue, orange, green) correspond to power settings yielding approximately the same mean microwave power input for both approaches: 140 W and 2 W/g, 200 W and 3 W/g, and 220 W and 3.2 W/g. **Panel A:** Adapted from Kalinke et al. (2024). **Panel B:** Fully original data from this study. * A minimum absolute power of 80 W was maintained. ** Only one successful repetition possible.

3.2.3, this increase in inhomogeneity can be attributed to shorter equilibration times due to faster drying at higher power levels. Additionally, higher power levels can lead to greater regional disparities in field strength, exacerbating temperature inhomogeneities.

There are two exceptions to this trend of increasing inhomogeneity with increasing power level. One was observed for the 220 W drying in the constant approach (Fig. 9 A): The temperature inhomogeneity for 220 W was lower than that for 200 W and 180 W. At this maximum power level of 220 W, drying occurred so rapidly that the transition stage—prone to inhomogeneities—was passed too quickly for significant temperature disparities to develop. This was discussed in detail in Kalinke et al. (2024). Therefore, an in-depth discussion of the constant approach is omitted here, as it only serves as a reference drying process for comparison reasons for the novel adjusted approach in this study. The other exception was observed during 1 W/g drying in the adjusted approach (Fig. 9 B). The temperature disparity for 1 W/g was slightly higher than for 2 W/g. This was due to the minimum power limitation of the MWFD equipment, which was set at 80 W. Near the end of drying, the actual microwave power input for 1 W/g could not decrease below this limit and remained at 80 W. At this stage, 80 W corresponded to approximately 2 W/g when calculated based on the final sample weight. This means that the actual power levels for both settings (1 W/g and 2 W/g) were nearly the same by the end of drying, leading to similar temperature disparities.

Overall, these exceptions do not contradict the general observation that higher microwave power results in a higher inhomogeneity.

2) Fig. 9 demonstrates that the adjusted power approach significantly reduced temperature inhomogeneity compared to the constant power approach. This becomes evident from the colour-coded temperature curves in Fig. 9A and B, where drying processes with equal $\overline{P}$ are highlighted with the same colour (blue, orange, green). Specific comparisons include 140 W (constant) vs. 2 W/g (adjusted), 200 W (constant) vs. 3 W/g (adjusted), and 220 W (constant) vs. 3.2 W/g (adjusted). The comparison between 220 W and 3.2 W/g has already been discussed in detail in section 3.2. These comparisons show that the adjusted power approach consistently resulted in lower maximum temperature oscillation spans than the corresponding constant power approach (*t*-test; $p < 0.05$). As hypothesised and already discussed in detail in section 3.2.3, this improved temperature uniformity can be attributed to the lower absolute power levels applied (effect 1 in section 3.2.3) during the inhomogeneity-prone later stages of MWFD (effect 2 in section 3.2.3).

Additional findings from Fig. 9 are that the colour-coded temperature curves in Fig. 9 A and B show that the constant approach resulted in substantially higher final product temperatures with equal $\overline{P}$. This finding was in line with Duan et al. (2012) in the context of their stepwise power-reduction approach. It was held responsible for the significantly lower product quality of apple crisps dried with the constant approach compared to a reducing power approach.

Another observation from Fig. 9 B concerns the progression of temperature inhomogeneity under the adjusted power approach. As previously discussed in Section 3.2.3, there was a characteristic rise and fall behaviour of temperature inhomogeneity for 3.2 W/g drying. While this behaviour was also seen for power levels exceeding 3.2 W/g in Fig. 9 B, this behaviour got less pronounced for decreasing microwave power levels. At 2 and 3 W/g, this rise and fall behaviour was only marginally apparent (at approx. 50 min). At 1 W/g, no rise and fall behaviour was evident. Instead, the progression of inhomogeneity in these cases became increasingly similar to that of a constant power approach drying at very low power levels.

As discussed in Section 3.2.3, the reduction in microwave power during drying was considered responsible for the observed fall in inhomogeneity. At lower P_{SET} levels in the adjusted approach, the absolute reduction in microwave power over the course of drying becomes smaller compared to higher power settings. This likely diminished the corresponding effect of falling inhomogeneity in the adjusted approach at low power settings. Consequently, at lower power settings (1–3 W/g), the inhomogeneity behaviour increasingly resembled that observed under constant power input at very low input power levels. At 1 W/g, the characteristic rise and fall in inhomogeneity was no longer evident. This was likely due to both, the minimal reduction in absolute power input and hardware limitations that prevented reduction of the microwave input power below 80 W.

Regardless of these differences in temporal inhomogeneity behaviour for different power settings, the adjusted power approach consistently led to lower overall temperature inhomogeneity compared to traditional MWFD using equivalent constant microwave power input.

3.4. Further considerations

When applying our newly developed adjusted approach to other

Table 2
Maximum temperature inhomogeneity for different settings of P_{SET} as derived from the temperature progression curves from Fig. 9; Arrows indicate a significant increase in data sets (*t*-test, $p < 0.05$); Font colours (blue, orange, green) indicate power settings yielding approximately the same mean microwave power input for both approaches. Constant power approach data derived from data from Kalinke et al. (2024). Adjusted power approach shows fully original data from this study. * A minimum absolute power of 80 W was maintained. ** Only one successful repetition possible.

Power approach	Set microwave power (P_{SET})	Maximum temperature inhomogeneity		
constant	120 W	13.9 ±0.5 °C		↓ Significant increase
	140 W	22.1 ±9.4 °C		
	160 W	43.3 ±2.1 °C		
	180 W	54.7 ±5.4 °C		
	200 W	53.5 ±9.8 °C		
	220 W	46.3 ±4.9 °C		
adjusted	1 W/g x m(t)	10.7 ±0.3 °C	*	↓ Significant increase
	2 W/g x m(t)	7.9 ±1.3 °C		
	3 W/g x m(t)	9.3 ±0.1 °C		
	3.2 W/g x m(t)	11.3 ±4.9 °C		
	4 W/g x m(t)	23.7 ±10.8 °C		
	5 W/g x m(t)	34.7 ±2.2 °C		
	6 W/g x m(t)	65.1 °C	**	

products, some potential limitations are to be considered: The sample must be capable of supporting the higher drying rates at the beginning of the process. If not, the increased maximum drying rates could result in vapour pressure buildup inside the product matrix and structural damage to the sample, as known from high constant microwave power drying (Kaysan et al., 2024; Ozcelik et al., 2019b). Additionally, shifting higher power inputs to the initial drying stage in the adjusted approach can lead to very high absolute power levels early in the process. These elevated power levels increase the risk of undesirable plasma formation (corona discharge) at the beginning of drying (Ambros et al., 2018; Duan et al., 2010, 2012). Plasma risk at the end of drying is reduced. Plasma formation is most likely at the beginning and in the end of MWFD (Duan et al., 2012). In the present study, excessively high product temperatures limited a further increase of microwave power, before structural damage or plasma did. It should be noted that also high final product temperatures, as observed for very high power levels even with the adjusted approach, are undesirable. They can negatively affect heat-sensitive, quality-determining components in the product. This could additionally be addressed by combining the adjusted approach with a temperature-controlled process control in the future.

4. Conclusion

A newly developed microwave power control strategy was tested for its capability to increase temperature uniformity compared to the conventional approach of constant microwave power input along drying. For this, absolute power input was constantly adjusted to the current sample weight instead of choosing a set constant absolute power input. Reduced microwave power input at the end of drying resulted in substantially more uniform temperature distributions at lower final product temperatures. High initial microwave input power compensated for slower drying due to reduced microwave power input at the end of drying. Hence, for the adjusted power approach, process uniformity was not a trade-off for time- and energy-efficiency. Moreover, for the same mean microwave power input along drying, the adjusted approach resulted in faster drying, lower total energy consumption and less microwave energy usage (approximately 15 %), while significantly reducing temperature inhomogeneity. This novel, adjusted power approach, therefore, presents a promising new power control strategy for MWFD processes. It was based on continuous weight monitoring of the sample. If this is not feasible, a straightforward alternative could be to steadily reduce the power along drying time.

The high power levels used in this study were specifically selected to explore the effects of both approaches under a broad experimental range. This was possible because the tested foam samples featured a highly porous structure, capable of supporting substantial mass transfer and enabling the exploration of a wide range of power settings. For other products, the applicable range of microwave power levels is expected to be narrower and consequently, is expected to fall within the range examined in this study. Of course, the best suited power level has to be selected in response to the individual product and task.

In this study, the adjusted approach was evaluated in combination with sample movement on a turntable. As sample movement—via rotation of turntables, drums or trays—is employed in all industrial-scale MWFD food applications known to the authors, this moved-sample configuration appears most relevant for industrial implementation. However, with the advent of novel solid-state microwave generators enabling dynamic microwave field variation, future investigations into the feasibility of the adjusted approach under stationary sample conditions with targeted microwave field variation may also be of interest. Additionally, combining the adjusted approach for high power levels with additional temperature control could offer a promising option for further improvement of process control. While process control is crucial, it should not be overlooked that the properties of the product itself are also important factors for improving efficiency and uniformity in MWFD. In conclusion, the proposed novel power control strategy should be further explored in the future, considering various product configurations and the effect of other methods to enhance uniformity, such as sample movement, frequency variation, and temperature control.

CRediT authorship contribution statement

Isabel Kalinke: Writing – review & editing, Writing – original draft, Visualization, Supervision, Project administration, Methodology, Investigation, Formal analysis, Data curation, Conceptualization. **Günther Unterbuchberger:** Investigation. **Ulrich Kulozik:** Writing – review & editing, Supervision, Resources, Project administration, Funding acquisition.

Declaration of AI and AI-assisted technologies in the writing process

During the preparation of this work the authors used ChatGPT (OpenAI, San Francisco, USA) and Microsoft Copilot (Microsoft Corporation, Redmod, USA) in order to improve readability. After using this tool, the authors reviewed and edited the content as needed and take full responsibility for the content of the publication.

Funding declaration

This research work was supported by funds from: The Federal Ministry of Food and Agriculture (BMEL) based on a decision of the Parliament of the Federal Republic of Germany via the Federal Office for Agriculture and Food (BLE) under the innovation support program (grant number 313.06.01-28-1-A1.053-16);

The program for promoting the Industrial Collective Research (IGF) of the German Federal Ministry for Economic Affairs and Climate Action (BMWK), based on a resolution of the German Parliament, via AiF, Cologne and FEI, Bonn, AiF-Project 22205N.

Declaration of competing interest

The authors declare that they have no known competing financial interests or personal relationships that could have appeared to influence the work reported in this paper.

Acknowledgement

We gratefully thank Marius Reiter for critical review of the manuscript and Johanna Röder for her support in data curation.

Data availability

Data will be made available on request.

References

Abbasi, S., Azari, S., 2009. Novel microwave-freeze drying of onion slices. Int. J. Food Sci. Technol. 44 (5), 974–979.
Ambros, S., Bauer, S.A.W., Shylkina, L., Foerst, P., Kulozik, U., 2016. Microwave-vacuum drying of lactic acid bacteria: influence of process parameters on survival and acidification activity. Food Bioprocess Technol. 9 (11), 1901–1911.
Ambros, S., Mayer, R., Schumann, B., Kulozik, U., 2018. Microwave-freeze drying of lactic acid bacteria: influence of process parameters on drying behavior and viability. Innov. Food Sci. Emerg. Technol. 48, 90–98.
Asokapandian, S., Venkatachalam, S., Swamy, G.J., Kuppusamy, K., 2016. Optimization of foaming properties and foam mat drying of muskmelon using soy protein. J. Food Process. Eng. 39 (6), 692–701.
Atuonwu, J., Tassou, S., 2018. Quality assurance in microwave food processing and the enabling potentials of solid-state power generators: a review. J. Food Eng. 234, 1–15.
Bengtsson, N.E., Risman, P.O., 1971. Dielectric properties of foods at 3 GHz as determined by a cavity perturbation technique. J. Microw. Power 6 (2), 107–123.
Datta, A.K., Anantheswaran, R.C. (Eds.), 2001. Handbook of Microwave Technology for Food Applications. Marcel Dekker Inc., New York.
Duan, X., Ren, G.Y., Zhu, W.X., 2012. Microwave freeze drying of Apple slices based on the dielectric properties. Dry. Technol. 30 (5), 535–541.
Duan, X., Zhang, M., Mujumdar, A.S., Wang, S., 2010. Microwave freeze drying of sea cucumber (*Stichopus japonicus*). J. Food Eng. 96 (4), 491–497.
Ferrão, T.S., Tischer, B., Menezes, M.F.S.C., Hecktheuer, L.H.R., Menezes, C.R., Barin, J. S., Michels, L., Wagner, R., 2017. Effect of microwave and hot air drying on the physicochemical characteristics and quality of jelly palm pulp. Food Sci. Technol. Res. 23 (6), 835–843.
Flores, A.A., Goff, H.D., 1999. Recrystallization in ice cream after constant and cycling temperature storage conditions as affected by stabilizers. J. Dairy Sci. 82 (7).
Gitter, J.H., Geidobler, R., Presser, I., Winter, G., 2018. Significant drying time reduction using microwave-assisted freeze-drying for a monoclonal antibody. J. Pharmaceut. Sci. 107 (10), 2538–2543.
Jiang, H., Zhang, M., Liu, Y., Mujumdar, A.S., Liu, H., 2013a. The energy consumption and color analysis of freeze/microwave freeze banana chips. Food Bioprod. Process. 91 (4), 464–472.
Jiang, H., Zhang, M., Mujumdar, A.S., 2010. Microwave freeze-drying characteristics of banana crisps. Dry. Technol. 28 (12), 1377–1384.
Jiang, H., Zhang, M., Mujumdar, A.S., Lim, R.-X., 2013b. Analysis of temperature distribution and SEM images of microwave freeze drying banana chips. Food Bioprocess Technol. 6 (5), 1144–1152.
Jiang, X., Kazarin, P., Sinanis, M.D., Darwish, A., Raghunathan, N., Alexeenko, A., Peroulis, D., 2022. A non-invasive multipoint product temperature measurement for pharmaceutical lyophilization. Sci. Rep. 12 (1), 12010.
Kaatze, U., Uhlendorf, V., 1981. The dielectric properties of water at microwave frequencies. Z. Phys. Chem. 126 (2), 151–165.
Kadam, D.M., Balasubramanian, S., 2011. Foam mat drying of tomato juice. J. Food Process. Preserv. 35 (4), 488–495.
Kalinke, I., Kubbutat, P., Taghian Dinani, S., Ambros, S., Ozcelik, M., Kulozik, U., 2022. Critical assessment of methods for measurement of temperature profiles and heat load history in microwave heating processes-A review. Compr. Rev. Food Sci. Food Saf. 1–31.
Kalinke, I., Kulozik, U., 2023. Irreversible thermochromic ink in the identification of over- and under-processed product segments in microwave-assisted freeze drying. J. Food Eng., 111470
Kalinke, I., Kulozik, U., 2024. Enhancing microwave freeze drying: exploring maximum drying temperature and power input for improved energy efficiency and uniformity. Food Bioprocess Technol. (17), 5357–5371.
Kalinke, I., Pusl, F., Häderle, F., Kulozik, U., 2023. A comparative study of frequency-shifting strategies for uniform and energy-efficient microwave heating in solid-state microwave systems. Innov. Food Sci. Emerg. Technol. 86, 103388.
Kalinke, I., Röder, J., Unterbuchberger, G., Kulozik, U., 2024. Microwave-assisted freeze drying: the role of power input and temperature control on energy efficiency and uniformity. J. Food Eng. 390, 112410.
Kaysan, T., Zhou, X., Gaukel, V., 2024. Process intensification of microwave-assisted freeze-drying by frequency adjustment in real-time using solid-state technology. J. Food Eng. 383, 112221.
Khalloufi, S., Robert, J.-L., Ratti, C., 2005. Solid foods freeze-drying simulation and experimental data. J. Food Process. Eng. 28 (2), 107–132.
Kubbutat, P., Kulozik, U., Dombrowski, J., 2021. Foam structure preservation during microwave-assisted vacuum drying: significance of interfacial and dielectric properties of the bulk phase of foams from polysorbate 80-Maltodextrin dispersions. Foods 10 (6).
Kubbutat, P., Tauchnitz, A., Kulozik, U., 2020. Water vapor pathways during freeze-drying of foamed product matrices stabilized by maltodextrin at different concentrations. Processes 8 (11), 1463.
Li, R., Huang, L., Zhang, M., Mujumdar, A.S., Wang, Y.C., 2014. Freeze drying of apple slices with and without application of microwaves. Dry. Technol. 32 (15), 1769–1776.
Marti, J., Mauersberger, K., 1993. A survey and new measurements of ice vapor pressure at temperatures between 170 and 250K. Geophys. Res. Lett. 20 (5), 363–366.
Mätzler, C., Wegmüller, U., 1987. Dielectric properties of freshwater ice at microwave frequencies. J. Phys. Appl. Phys. 20 (12), 1623–1630.
Morgan, S.P., 1949. Effect of surface roughness on eddy Current losses at microwave frequencies. J. Appl. Phys. 20 (4), 352–362.
Oliveira, M., Franca, A.S., 2002. Microwave heating of foodstuffs. J. Food Eng. 53, 347–359.
Ozcelik, M., Ambros, S., Heigl, A., Dachmann, E., Kulozik, U., 2019a. Impact of hydrocolloid addition and microwave processing condition on drying behavior of foamed raspberry puree. J. Food Eng. 240, 83–91.
Ozcelik, M., Heigl, A., Kulozik, U., Ambros, S., 2019b. Effect of hydrocolloid addition and microwave-assisted freeze drying on the characteristics of foamed raspberry puree. Innov. Food Sci. Emerg. Technol. 56, 102183.
Ozkan, I.A., Akbudak, B., Akbudak, N., 2007. Microwave drying characteristics of spinach. J. Food Eng. 78 (2), 577–583.
Pikal, M.J., 1994. Freeze-drying of proteins: process, formulation, and stability. In: Formulation and Delivery of Proteins and Peptides. American Chemical Society, Washington, DC, pp. 120–133.
Qadri, O.S., Osama, K., Srivastava, A.K., 2020a. Foam mat drying of papaya using microwaves: machine learning modeling. J. Food Process. Eng. 43 (6).
Qadri, O.S., Srivastava, A.K., Yousuf, B., 2020b. Trends in foam mat drying of foods: special emphasis on hybrid foam mat drying technology. Crit. Rev. Food Sci. Nutr. 60 (10), 1667–1676.
Raharitsifa, N., Ratti, C., 2010. Foam-mat freeze-drying of apple juice: part 1: experimental data and ANN simulations. J. Food Process. Eng. 33 (s1), 268–283.
Regier, M., Knoerzer, K., Schubert, H. (Eds.), 2017. The Microwave Processing of Foods. Elsevier, Cambridge.
Rzepecka, M.A., Brygidyr, A.M., McConell, M.B., 1976. Foam-mat dehydration of tomato paste using microwave energy. Can. Agric. Eng. 18 (1).
Sankat, C.K., Castaigne, F., 2004. Foaming and drying behaviour of ripe bananas. LWT - Food Sci. Technol. (Lebensmittel-Wissenschaft -Technol.) 37 (5), 517–525.
Sarciaux, J.M., Mansour, S., Hageman, M.J., Nail, S.L., 1999. Effects of buffer composition and processing conditions on aggregation of bovine IgG during freeze-drying. J. Pharmaceut. Sci. 88 (12), 1354–1361.
Schmidt, F., Graf, B., Hinrichs, J., Kern, C., 2022. Continuous microwave-assisted extrusion for high moisture texturized foods: a feasibility study. Innov. Food Sci. Emerg. Technol. 78, 103020.
Sickert, T., Bergmann, R., Chistoph, J., Gaukel, V., 2023a. A time-saving approach to parameter studies in microwave-assisted freeze drying. Processes 11 (10), 2886.
Sickert, T., Kalinke, I., Christoph, J., Gaukel, V., 2023b. Microwave-assisted freeze-drying with frequency-based control concepts via solid-state generators: a simulative and experimental study. Processes 11 (2), 327.
Smith, G., Arshad, M.S., Polygalov, E., Ermolina, I., 2014. Through-vial impedance spectroscopy of the mechanisms of annealing in the freeze-drying of maltodextrin:

the impact of annealing hold time and temperature on the primary drying rate. J. Pharmaceut. Sci. 103 (6), 1799–1810.
Sunderland, J.E., 1980. Microwave freeze drying. J. Food Process. Eng. 4 (4), 195–212.
Taghian Dinani, S., Kubbutat, P., Kulozik, U., 2020. Assessment of heating profiles in model food systems heated by different microwave generators: solid-state (semiconductor) versus traditional magnetron technology. Innov. Food Sci. Emerg. Technol. 63, 102376.
Tang, X., Pikal, M.J., 2004. Design of freeze-drying processes for pharmaceuticals: practical advice. Pharm. Res. 21 (2), 191–200.
Valenzuela, C., Aguilera, J.M., 2013. Aerated Apple leathers: effect of microstructure on drying and mechanical properties. Dry. Technol. 31 (16), 1951–1959.
van der Merwe, J.P., Swardt, J.B. de, 2017. Power control of a domestic microwave oven. In: 2017 IEEE Africon. IEEE, Cape Town, pp. 574–578, 18.09.2017 - 20.09.2017.
Wang, J., Xi, Y.S., 2005. Drying characteristics and drying quality of carrot using a two-stage microwave process. J. Food Eng. 68 (4), 505–511.
Wang, R., Zhang, M., Mujumdar, A.S., Sun, J.-C., 2009. Microwave freeze–drying characteristics and sensory quality of instant vegetable soup. Dry. Technol. 27 (9), 962–968.
Wang, W., Zhao, C., Sun, J., Wang, X., Zhao, X., Mao, Y., Li, X., Song, Z., 2015. Quantitative measurement of energy utilization efficiency and study of influence factors in typical microwave heating process. Energy 87, 678–685.
Yang, H.W., Gunasekaran, S., 2001. Temperature profiles in a cylindrical model food during pulsed microwave heating. Food Engineering and Physical Properties 66 (7), 998–1004.
Yang, H.W., Gunasekaran, S., 2004. Comparison of temperature distribution in model food cylinders based on Maxwell's equations and Lambert's law during pulsed microwave heating. J. Food Eng. 64 (4), 445–453.
Yang, R., Chen, J., 2022. Dynamic solid-state microwave defrosting strategy with shifting frequency and adaptive power improves thawing performance. Innov. Food Sci. Emerg. Technol. 81, 103157.
Yang, R., Chen, J., 2024. Heating performance of dual-source microwave heating using different frequency shifting strategies in a solid-state system. Food Res. Int. 175, 113781.
Zhang, G., Leparoux, S., Liao, H., Coddet, C., 2006a. Microwave sintering of poly-ether-ether-ketone (PEEK) based coatings deposited on metallic substrate. Scr. Mater. 55 (7), 621–624.
Zhang, H., Datta, A.K., 2003. Microwave power absorption in single - and multiple-item foods. Food Bioprod. Process. 81 (3), 257–265.
Zhang, M., Tang, J., Mujumdar, A.S., Wang, S., 2006b. Trends in microwave-related drying of fruits and vegetables. Trends Food Sci. Technol. 17 (10), 524–534.
Zhang, Z., Su, T., Zhang, S., 2018. Shape effect on the temperature field during microwave heating process. J. Food Qual. 2018, 1–24.
Zhou, X., Tang, Z., Pedrow, P.D., Sablani, S.S., Tang, J., 2023. Microwave heating based on solid-state generators: new insights into heating pattern, uniformity, and energy absorption in foods. J. Food Eng. 357, 111650.